ENVIRONMENTAL RESEARCH
LETTERS

LETTER • OPEN ACCESS

Southern Hemispheric jet swing linked to Arctic stratospheric polar vortex

To cite this article: Fei Xie *et al* 2024 *Environ. Res. Lett.* **19** 044053

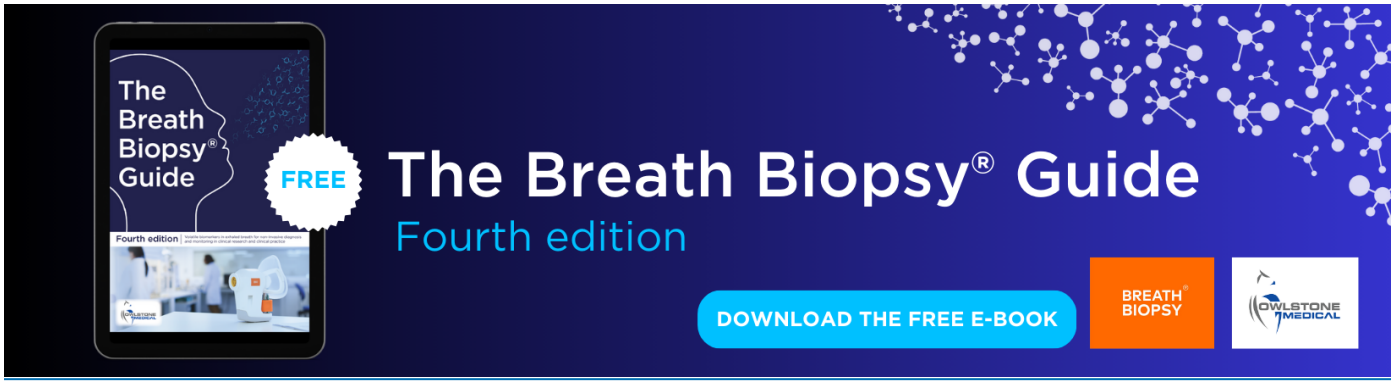

IOP Publishing Environ. Res. Lett. 19 (2024) 044053 https://doi.org/10.1088/1748-9326/ad3460

ENVIRONMENTAL RESEARCH
LETTERS

OPEN ACCESS

RECEIVED
6 December 2023

REVISED
21 February 2024

ACCEPTED FOR PUBLICATION
15 March 2024

PUBLISHED
28 March 2024

LETTER

Southern Hemispheric jet swing linked to Arctic stratospheric polar vortex

Fei Xie[1], Xuan Ma[1,*], Yanjie Li[2], Jianping Li[3], Xiaosong Chen[1,*], Wenshou Tian[4], Cheng Sun[1], Mian Xu[4], Jiankai Zhang[4], Ke Gui[5], Ruiqiang Ding[1], Yan Xia[1] and Yingli Niu[1]

[1] School of Systems Science/Key Laboratory of Environmental Change and Natural Disasters of Chinese Ministry of Education/College of Global Change and Earth System Science, Beijing Normal University, Beijing, People's Republic of China
[2] State Key Laboratory of Numerical Modeling for Atmospheric Sciences and Geophysical Fluid Dynamics, Institute of Atmospheric Physics, Chinese Academy of Sciences, Beijing, People's Republic of China
[3] Frontiers Science Center for Deep Ocean Multispheres and Earth System (FDOMES)/Key Laboratory of Physical Oceanography/Institute for Advanced Ocean Studies, Ocean University of China, Qingdao, People's Republic of China
[4] Key Laboratory for Semi-Arid Climate Change of the Ministry of Education, College of Atmospheric Sciences, Lanzhou University, Lanzhou, People's Republic of China
[5] State Key Laboratory of Severe Weather & Key Laboratory of Atmospheric Chemistry of CMA, Chinese Academy of Meteorological Sciences, Beijing, People's Republic of China
[*] Authors to whom any correspondence should be addressed.

E-mail: maxuan@bnu.edu.cn and chenxs@bnu.edu.cn

Keywords: Arctic stratospheric polar vortex (APV), Southern Hemispheric jet, planetary waves, precipitation

Supplementary material for this article is available online

Abstract

Our study reframes our understanding of stratosphere–troposphere interactions, traditionally thought to be confined within individual hemispheres, by introducing a novel cross-hemispheric link. We demonstrate that strong boreal winter Arctic stratospheric polar vortex (APV) boosts the transmission of upper tropospheric waves from Northern Hemisphere's mid-high latitudes to the equator. Facilitated by the tropical central and eastern Pacific's 'westerly bridge', these waves reach Southern Hemisphere's mid-high latitudes. The entire process shows a 'semicircular road'. Waves reaching the Southern Hemisphere affect the circulation through wave-flow interaction, causing a southward swing of the Southern Hemispheric westerly jet center. This displacement weakens the subtropical jet and strengthens the polar jet, resulting in increased subtropical precipitation and decreased mid-latitude precipitation in the Southern Hemisphere during austral summer. Correspondingly, a weak APV may lead to the opposite result. Our findings underscore APV's broader impact on the tropospheric atmosphere, extending beyond prior knowledge.

1. Introduction

The stratospheric polar vortex plays a pivotal role in stratosphere–troposphere interactions. In the Northern Hemisphere, the Arctic stratospheric polar vortex (APV) (Waugh *et al* 2017, Mitchell *et al* 2021) forms in autumn, peaks in winter, and decays by early spring, with the strongest variability from January to March (supplementary figure S1). APV alterations, such as strengthening due to ozone depletion or weakening from stratospheric sudden warming, deeply impact Northern Hemisphere's surface climate (Haynes *et al* 1991, Baldwin and Dunkerton 2001, Ambaum and Hoskins 2002, Thompson *et al* 2006, Domeisen and Butler 2020, Baldwin *et al* 2021, Scaife *et al* 2022, Tian *et al* 2023). For example, the APV's crucial role in modulating the Arctic Oscillation (Baldwin and Dunkerto 1999, Black 2002); variations in APV phases correlate with the North Atlantic Oscillation (Limpasuvan *et al* 2005, Charlton-Perez *et al* 2018, Domeisen 2019), leading to abnormal temperature fluctuations in mid-latitudes (Scaife *et al* 2008, Kolstad *et al* 2010, Butler *et al* 2017, King *et al* 2019). These changes can influence surface weather for weeks to months (Hartmann 1981, Moulin *et al* 1997, Kidston *et al* 2015, Xie *et al* 2018, Ma *et al* 2019, Afargan-Gerstman and Domeisen 2020) and even impact the North Atlantic Ocean meridional overturning circulation (Reichler *et al* 2012), as well as the tropical El Niño-Southern Oscillation (ENSO) (Xie

et al 2016). However, the traditional paradigm that stratospheric–tropospheric interactions are thought to be constrained to individual hemispheres.

In the Southern Hemisphere, researches indicate stratospheric ozone-induced Antarctic stratospheric polar vortex changes drive the Southern Hemispheric westerly jet trend during austral summer (Gillett and Thompson 2003, Perlwitz *et al* 2008, Son *et al* 2008). This jet significantly influences regional climate, affecting precipitation (Feldstein 2011, Kang *et al* 2011), Australian wildfires (Lim *et al* 2019), surface temperature (Thompson *et al* 2011), sea ice extent (Thompson and Solomon 2002), storm track variability (Yin 2005), and arid region locations (Lu *et al* 2007). A previous study observed potential interhemispheric synchronization of the Arctic Oscillation and the Antarctic Oscillation in February (Tachibana *et al* 2018). Given the APV's crucial role in modulating the Arctic Oscillation (Baldwin and Dunkerto 1999, Black 2002), it prompts the question: can significant APV fluctuations cross the equator and influence the Southern Hemisphere's atmospheric circulation?

2. Data and experiments

2.1. Data

In this study, we leveraged an array of datasets encompassing the European Centre for Medium-Range Weather Forecasts Reanalysis v5 (ERA5) (Hersbach *et al* 2020, Bell *et al* 2021), the Japanese 55 year Reanalysis (JRA-55) (Kobayashi *et al* 2015), and the Global Precipitation Climatology Project (GPCP) (Adler *et al* 2018). The ERA5, featuring a $1^\circ \times 1^\circ$ spatial resolution, monthly data span the period 1950–2022 and daily data span the period 1950–2022. Conversely, the JRA-55, characterized by a $2.5^\circ \times 2.5^\circ$ resolution, daily data cover the years 1958–2022. Additionally, we adopted version 2.3 of the monthly GPCP dataset, which has a $2.5^\circ \times 2.5^\circ$ resolution and encapsulates the period 1979–2022.

2.2. Model and simulation

The present study employed the Community Atmosphere Model version 6 (CAM6), a key component of the Community Earth System Model version 2.2 (CESM2.2), a comprehensive coupled climate system model. CAM6 incorporates a finite-volume dynamical core with 32 vertical tiers stretching from the surface to 3 hPa. The simulations were carried out at a resolution of $1.9^\circ \times 2.5^\circ$ (latitude × longitude). It is pivotal to note that CAM primarily targets tropospheric simulations. Within the scope of this study, stratospheric simulations are largely confined to the modeling of the stratospheric polar vortex, eschewing the impact of other stratospheric processes on the mechanism. The principal altitude range for mechanism simulation remains within the troposphere. Hence, the employment of the CAM model in this investigation is deemed appropriate.

This study features 13 experiments, segmented into three categories. Group 1 consists of the Ctrl experiment (Ctrl) and eight nudging experiments (SA_20 and WA_20, SA_30 and WA_30, SA_50 and WA_50, SA_80 and WA_80), all of which probe the Southern Hemisphere climate's reaction to fluctuations in the intensity of the Arctic Stratospheric Polar Vortex (APV). Group 2 encompasses two nudging experiments (SHW_SS and SHW_NS) that investigate the repercussions of changes in the Southern Hemispheric westerly jet on APV amplitude. Meanwhile, Group 3 entails two nudging experiments (SA_FWD and WA_FWD) which ascertain how the Southern Hemispheric climate adapts to deviations in APV strength when zonal winds in the tropical central and eastern Pacific westerly area remain static. Comprehensive experimental blueprints are outlined in supplementary tables S1–3 in the ensuing experimental delineation.

For all iterations, nudging is executed eight times daily, specifically at 0, 3, 6, 9, 12, 15, 18, and 21 o'clock. The zonal wind used for nudging is the 3D zonal wind, with a nudging intensity set at 100%. This means that within the zonal wind's nudged region, the model's zonal wind precisely mirrors the given zonal wind, unaffected by any other dynamic processes during the simulation.

3. Results

3.1. Southern Hemispheric jet and precipitation linked to APV anomaly

Figures 1(a)–(c) depicts the correlation coefficients between the Arctic Stratospheric Polar Vortex Intensity Index (APVI) and global zonal-mean zonal wind alterations from January to March based on ERA5 daily data from 1979–2022. Considering the time of atmospheric signal propagation, the global zonal wind changes here are delayed by 15 d compared to APVI. Our analysis reveals a significant inverse correlation between APVI and the northern branch of the Southern Hemispheric westerly jet (subtropical jet) during February and March (figures 1(b) and (c)). Simultaneously, a positive correlation exists with the southern branch of the westerly jet (polar jet). This suggests that the intensification and weakening of boreal winter APV align with the Southern Hemispheric westerly jet center's southerly and equatorial swings during austral summer, respectively. This pattern, primarily pronounced in February, is not evident in January (figure 1(a)). Moreover, from the altitude range of 200–300 hPa in figures 1(b) and (c), we can observe a wave train from the mid-high latitudes of the Northern Hemisphere to the mid-high latitudes of the Southern Hemisphere.

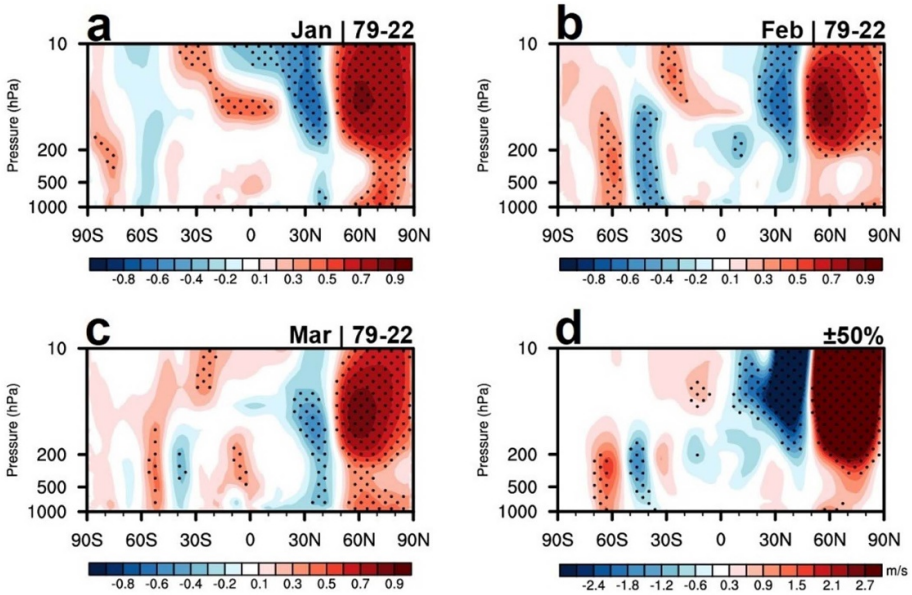

Figure 1. Exploring the correlations between the Arctic stratospheric polar vortex strength and variations in the Southern Hemispheric circulation. (a) Depiction of the correlation coefficient between the Arctic stratospheric polar vortex index (APVI) from 1–14 January and zonal-mean zonal wind fluctuations from 15–28 January, spanning 1979–2022, drawn from ERA5 daily datasets. (b) Analogous to (a), this frame captures February. (c) A reflection of (a), highlighting the interval of March. For context, the APVI within this research framework is characterized by zonal wind anomalies aggregated across the domain: 10–50 hPa, 180° W–180° E, and 60° N–70° N. (d) Simulated February zonal-mean zonal wind anomalies resulting from variations in APV strength 50% APV changes. The anomalies are obtained by SA_50 subtracting WA_50, as outlined in supplementary table S1. Areas pinpointed by dots signify statistical significance, gauged at the 95% confidence threshold, as determined by the Student's *t*-test.

When the research period of the ERA5 data is extended from 1979–2022 (44 years, figure 1(b)) to 1950–2022 (73 years, supplementary figure S2(a)), the correlation between APVI and the changes in the northern branch of the Southern Hemispheric westerly jet (subtropical jet) surpassed the 95% significance test. Note that, the correlation coefficient between the changes in the southern branch of the westerly jet (polar jet) and APVI did not pass the 95% significance test. We find that there is an extreme anomaly of polar jet (orange line, supplementary figure S2(c)) compared with subtropical jet (blue line, supplementary figure S2(c)) for the period from 1960 to 1970. If excluding this period from 1950–2022, the correlation between APVI and polar jet variations is also significant at 95% confident level (supplementary figure S2(b)). The correlation between APVI and Southern Hemispheric westerly jet from 1979 to 2022 based JRA-55 data agrees well with that of ERA5 (supplementary figure S3 and figures 1(a)–(c)). As the reanalysis data prior to 1979 did not assimilate enough observations (Bell *et al* 2021), we will select the 1979–2022 (44 years) as our research period hereafter.

To demonstrate the causal relationship between APV and changes in the intensity of the Southern Hemispheric westerly jet, we conducted several sensitivity experiments using the CAM6 climate model. The experiments aim to strengthen and weaken APV (supplementary table S1). The first set of experiments in supplementary table S1 used the nudging zonal wind method to strengthen and weaken APV, presented for 20%, 30%, 50%, and 80% changes in APV (supplementary table S1 and figure S4). These four variation amplitudes are less than or close to one standard deviation of APV intensity change. Figure 1(d) and supplementary figure S5 display the simulated results of abnormal changes in zonal wind between the strong and weak APV event experiments (supplementary table S1). By comparing the observational and simulated results (figures 1(b) and (d)/supplementary figure S5), we deduce that simulations altering APV at 50% and 80% intensities can reproduce the significant connection between APV and the observed Southern Hemispheric westerly jet changes in the observed data (figure 1(d) and supplementary figure S5(c)), but alterations at 20% and 30% intensities cannot (supplementary figures S5(a) and (b)). This indicates that changes in APV intensity can indeed force the swing phenomenon in the Southern Hemisphere westerly jet; only when APV intensity changes reach around 50% or more can there be significant changes in the Southern Hemisphere westerly jet. The experimental results not only simulate the impact of APV changes on the Southern Hemisphere westerly jet but also clearly illustrate a wave train connected to APV changes, spanning from the mid-high latitudes of the Northern Hemisphere to the mid-high

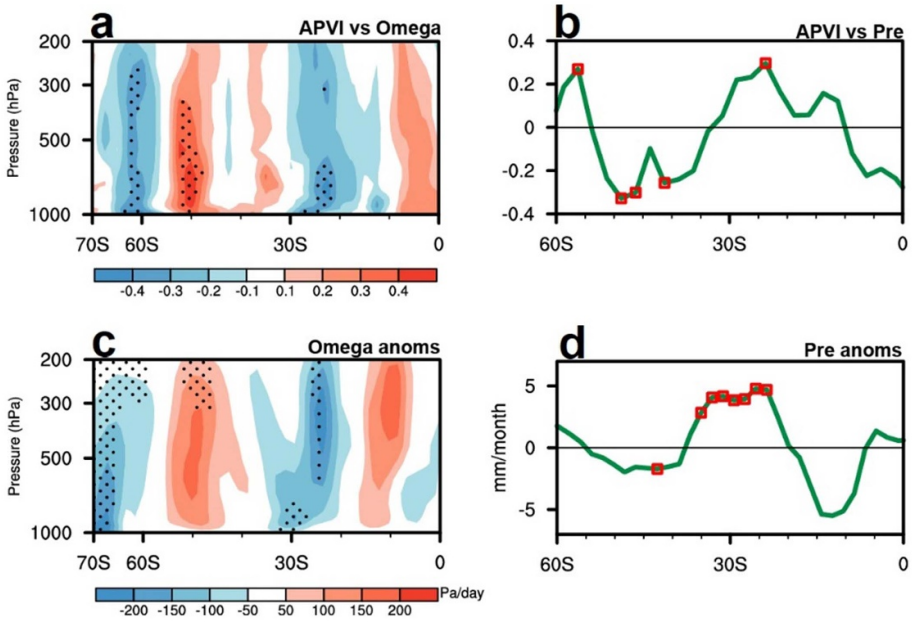

Figure 2. Assessing the ripple effects of the Arctic stratospheric polar vortex on precipitation patterns in the Southern Hemisphere. (a) Depiction of the correlation coefficient between the APVI from 1–14 February and zonal-mean omega fluctuations from 15–28 February, spanning 1979–2022, drawn from ERA5 daily datasets. (b) A representation of the February zonal-mean precipitation, crafted using the same comparative methodology as in (a). The omega values are extrapolated from the ERA5 daily dataset, while precipitation insights hail from the GPCP monthly dataset, with both spanning the timeframe of 1979–2022. (c)–(d) These panels illustrate the simulated anomalies discerned between the strong APV event experiment (SA_50) and its weaker counterpart (WA_50), as delineated in supplementary table S1. Specifically, (c) the zonal-mean omega, whereas (d) the zonal-mean precipitation. Regions earmarked by dots in (a), (c) and squares in (b), (d) validate statistical significance at the 95% confidence interval, corroborated by the Student's *t*-test.

latitudes of the Southern Hemisphere (figure 1(d)), and this is also evident in the observational results (figure 1(b)). Notably, the latitudinal wind change magnitude due to an 80% change in APV (supplementary figure S5(c)) is not more pronounced than that caused by a 50% change in APV (figure 1(d)). This nonlinear outcome will be a subject of further discussion in the future.

Strong APV events result in the attenuation of the northern branch of the Southern Hemispheric westerly jet and the amplification of the southern branch, prompting the jet center to lean towards the South Pole. This poleward repositioning of the extratropical jet aligns with the corresponding poleward movement of the Hadley and Ferrel cells' subtropical edge, as illustrated by the convergence and divergence of wave momentum fluxes along their polar and equatorial margins respectively (Kang *et al* 2011, Hu *et al* 2019). Figure 2(a) depicts the zonal-mean omega variations related to strong and weak APV occurrences based on ERA5. Intense APV events incite anomalous upwelling between 25° S–35° S and anomalous downwelling from 40° S–55° S (figure 2(a)). As a result, increased and decreased precipitation is registered around 30° S and 45° S, respectively, as inferred from GPCP datasets (figure 2(b)). Upon juxtaposing the observational and simulated data (figures 2(a)–(d)), it is discerned that the simulations nudging APV strength aptly mirror the bond between APV and the fluctuations in the Southern Hemispheric zonal-mean omega and rainfall observed empirically.

3.2. The 'semicircular road' of APV influencing Southern Hemisphere through 'westerly bridge'

Throughout the boreal winter, an upper-tropospheric westerly expanse emerges over the tropical central and eastern Pacific in the Northern Hemisphere (figure 3(a)). From the vertical cross-sectional diagram, it is evident that the tropical westerlies function akin to a bridge, seamlessly interlinking the atmospheric dynamism of the Northern and Southern Hemispheres (figure 3(b)). Previous researches emphasized that this westerly domain facilitates the transference of Northern Hemispheric waves to the Southern Hemisphere (Webster and Holton 1982, Hoskins and Ambrizzi 1993, Enomoto and Matsuda 1999, Li *et al* 2019). Our probing into the primary spatial patterns of tropospheric zonal wind variations (at elevations of 200–300 hPa, 400–500 hPa, and 600–700 hPa) via the Empirical Orthogonal Function (EOF) unveils a wave train configuration extending from the North Pacific to the South Pacific at 200–300 hPa (figure 3(c)).

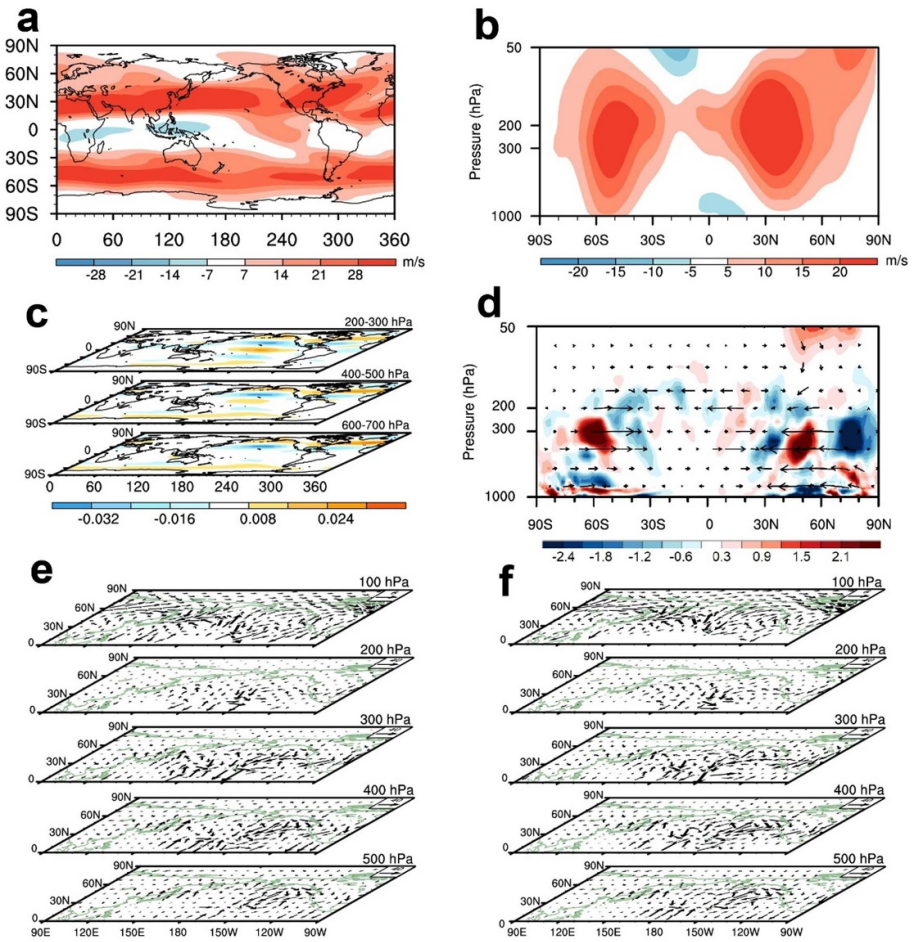

Figure 3. Elucidating the conduit through which the Arctic stratospheric polar vortex modulates the Southern Hemisphere. The depiction of the climatological zonal wind, (a) averaged over pressures 200–300 hPa, and (b) the zonal-mean (180–60° W) zonal wind climatology—both harnessed from the ERA5 monthly dataset for February. (c) The first leading mode procured from the Empirical Orthogonal Function (EOF) analysis, executed on the zonal wind at pressure intervals: 200–300 hPa, 400–500 hPa, and 600–700 hPa, leveraging ERA5 monthly data for February. (d) Composite anomalies in the E-P flux and its divergence/convergence, canvassed between February, for the spectrum of APV events (both strong and weak) extracted from ERA5 daily data. Vector arrows annotate the magnitude and bearing of the wave components. Notably, the E-P flux's divergence/convergence is delineated at intervals of ± 0.3 m s d^{-1}, with acceleration showcased in blue and deceleration in red. (e) Composite anomalies of the 3D wave flux (computed using the methodology of Takaya and Nakamura 2001) for February between strong and weak APV events at multiple pressure levels (100, 200, 300, 400, and 500 hPa) sourced from ERA5 daily data. Again, vector arrows designate the magnitude and trajectory of the wave constituents. (f) A parallel exploration as that in (e), albeit derived from the JRA-55 daily dataset. Anomalies in panels (d)–(f) are the result of juxtaposing February dominant APV events (where APVI exceeds 1SD) against their weaker counterparts during the same timeframe (APVI below—1SD). The analyses span the period from 1979 to 2022.

The mid-to-high latitudes of the Northern Hemisphere encounter the strongest baroclinic atmosphere during the boreal winter, generating numerous tropospheric waves. While one wave moves from mid-to-high latitudes towards the equator, another ascends into the stratosphere. These waveguides exhibit interannual variations in opposing directions, indicating that the strengthening of the equator-bound waveguide in the upper troposphere coincides with a weak polar waveguide. Previous studies documented that during episodes of intensified APV, the associated stratospheric wave flux is downward implying anomalously low wave activity as the vortex strengthens further via thermal relaxation. Below 100 hPa, anomalous wave fluxes are most intense and directed equatorward (strong anomalous poleward momentum flux) in the upper troposphere (Limpasuvan *et al* 2005). These waves are then possibly transmitted to the Southern Hemisphere through the Pacific's westerly bridge (figures 3(a) and (b)). Figure 3(d) illustrates the composite anomalies of the E-P flux along with their divergence between strong and weak APV events. As observed in figure 3(d), the divergence anomalies of the E-P flux display a characteristic semicircular road. This begins from mid-to-high latitudes of the Northern Hemisphere's troposphere, passes through the high-altitude tropical troposphere (200–300 hPa), and leads to the mid-to-high latitudes of the Southern Hemisphere's troposphere. The vector

arrows of the E-P flux on this semicircular road indicate a possible transfer of anomalous wave flux from the Northern Hemisphere through the westerly bridge to the Southern Hemisphere. The influx of Northern Hemispheric eddy momentum fluxes into the Southern Hemisphere results in the southward swing of the eddy-driven jet by wave-flow interaction (Webster and Holton 1982, Kang *et al* 2011, Hu *et al* 2019), thereby influencing the distribution of the westerly jet. Specifically, the anomalous convergence of the E-P flux in the Southern Hemisphere primarily occurs around 40° S, while the anomalous divergence mainly takes place near 60° S. This is consistent with the observed deceleration of the northern branch and acceleration of the southern branch of the Southern Hemispheric westerly jet stream, implying a poleward swing of the jet stream's center.

To better illustrate the anomalies in the Northern Hemisphere's wave flux caused by APV anomalies and determine their possible propagation to the Southern Hemisphere, we employed data sets from ERA5 and JRA-55, using the method of Takaya and Nakamura (2001) (refer to supplementary methods), we diagnosed this issue by calculating the 3D wave activity flux. Figures 3(e) and (f) presents the composite anomalies of the 3D wave flux vector for strong versus weak APV events based on ERA5 and JRA-55 datasets. Observations highlight the wave flux from the Northern Hemisphere's mid-latitudes (30° N–60° N), within 180–60° W longitude, displaying an anomalous southward propagation, especially prominent at the 200 hPa and 300 hPa levels. These results suggest that wave activity anomalies from the Northern Hemisphere, attributed to APV, may traverse the tropical westerly bridge to the Southern Hemisphere.

Supplementary figure S6 illustrates the propagation pathways of atmospheric disturbance-induced waves 1–5 trains from mid-high latitudes of the Northern Hemisphere in the upper troposphere, employing the wave ray method (refer to supplementary Methods). This method is akin to the pathways of wave energy propagation at group velocity and aptly captures the real-time transmission of atmospheric wave flux. Originating between 30° N–60° N and 150° E–120° W in the upper troposphere, our analysis revealed that waves 1–5 disturbances consistently reach mid-to-high latitudes in the Southern Hemisphere by February. Theoretically, we demonstrate that large-scale waves can traverse through the westerly bridge to the Southern Hemisphere. As seen in supplementary figures S6(a)–(e), with an increasing wave number, the sources of disturbances (depicted as black points in the figure) diminish. This reduction is attributed to the decreasing regions capable of generating meridional transmitting waves as the wave number escalates. Supplementary figure S7 portrays composite 200–300 hPa zonal wind anomalies between strong and weak APV events in February. A strong APV correlates with significant westerly anomalies north of 60° N and pronounced easterly anomalies between 30° N–60° N in the troposphere. This corresponds to the northward swing of the Northern Hemisphere's eddy-driven jet. A clear wave train crossing the equator is also discernible over the tropical central and eastern Pacific. In the Southern Hemisphere's mid-to-high latitudes, especially over the South Pacific, westerly anomalies are observed south of 60° S, and easterly anomalies north of 60° S, indicative of the westerly jet center's southward shift. Given the robust response of the South Pacific's westerly winds to APV, significant response signals have been noted for the Southern Hemisphere's zonal mean westerly winds (figure 1). Supplementary figure S7(b) presents the simulated result of abnormal changes in the upper tropospheric zonal wind between strong and weak APV events (SA_50 and WA_50 experiments, supplementary table S1), which aligns with observed results (supplementary figure S7(a)).

The second set of sensitivity experiments presented in supplementary table S2 sought to explore the potential influence of swing in the Southern Hemispheric westerly jet center—both southward and northward—on significant modifications in APV (supplementary table S2 and figure S8). Figure 4(a) showcases the simulated outcomes of abnormal zonal-mean zonal wind changes between experiments associated with southward and northward deviations of the Southern Hemispheric westerly jet center. The findings suggest that the intensity swings in the Southern Hemisphere westerly jet do not substantially influence APV.

To further corroborate the key bridging role of westerlies over the tropical Pacific—as proposed in our study—during the influence of APV anomalies on the Southern Hemispheric westerly jet, we delved into a third set of experiments. This set examined the implications of APV intensity variations on the Southern Hemisphere's circulation while inhibiting the wave flux transmission via the westerly bridge (supplementary table S3 and figure S9). Here we selected APV 50% variation as the research object. Figure 4(b) represents the simulated zonal-mean zonal wind anomalies between the strong and weak APV event experiments, with a constant zonal wind nudged in the tropical westerly region (SA_FWD and WA_FWD experiments, supplementary table S3). Our analysis infers that when a steady zonal wind prevails over the tropical central and eastern Pacific, the Southern Hemispheric westerly jet offers a minimal and insignificant response to APV anomalies (figure 4(b)). Such results emphasize the important role of the westerly bridge spanning the tropical central and eastern Pacific in moderating the influence of APV on the Southern Hemisphere's atmospheric dynamics.

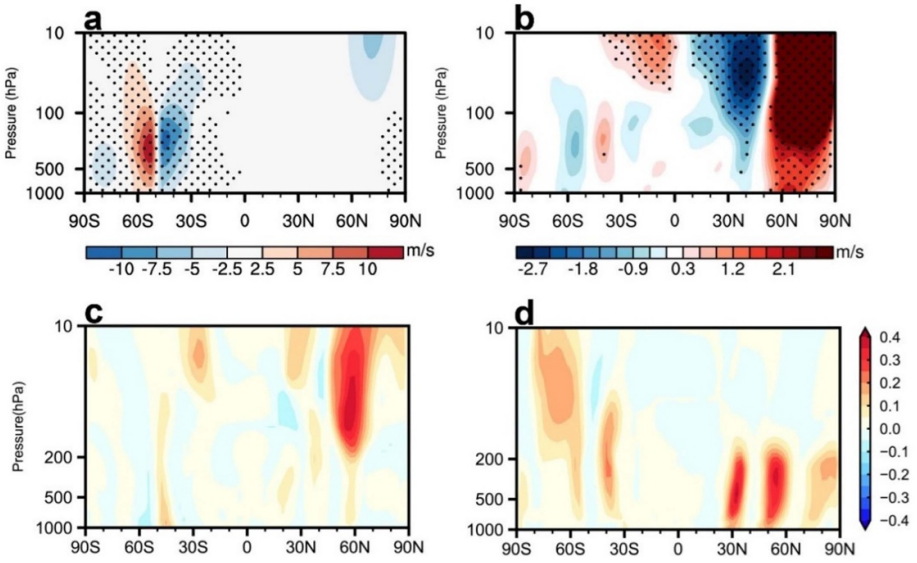

Figure 4. (a) Simulated February zonal-mean zonal wind anomalies resulting from variations in Southern Hemispheric Westerly strength. Anomalies in simulated zonal-mean zonal wind between the Westerly Southward Swing (SHW_SS) and Westerly Northward Swing (SHW_NS) experiments, as detailed in supplementary table S2. (b) Anomalies in simulated zonal-mean zonal wind under fixed westerly bridge conditions. Anomalies in simulated zonal-mean zonal wind between the strong APV event (SA_FWD) and weak APV event (WA_FWD) experiments, under fixed westerly bridge conditions over the tropical central and eastern Pacific, as described in supplementary table S3. Areas marked with dots indicate statistical significance at the 95% confidence level, evaluated using the Student's *t*-test. (c) Information flow from the 1–7 February APVI to 7–13 February zonal-mean zonal wind variations. (d) As in (c), but for 1–7 February Northern Hemisphere mid-to-high latitude zonal wind (average 300–400 hPa, 180° W–180° E, and 60° N–70° N) to 7–13 February zonal-mean zonal wind variations. Analyses utilize the ERA5 daily datasets from 1979 to 2022.

Due to the presence of the westerly bridge, it is plausible that changes in the Northern Hemisphere's tropospheric circulation can simultaneously affect the Arctic Polar Vortex (APV) and the Southern Hemisphere's circulation. The relationship we have found in our article between the APV and the Southern Hemisphere's westerly jet stream could be due to the APV's changes influencing the Northern Hemisphere's tropospheric circulation, which then impacts the Southern Hemisphere through the westerly bridge, or it could be that changes in the Northern Hemisphere's tropospheric circulation simultaneously affect the APV and the Southern Hemisphere. Here, using daily ERA5 data, we discuss the relationship between the February APV, Northern Hemisphere tropospheric circulation, and Southern Hemisphere tropospheric circulation through a lead-lag correlation analysis.

Supplementary figure S10 shows the correlation distribution of the February APV index with the global zonal mean U at 0, 2, 4, 6, 8, and 10 d lag. Based on supplementary figure S10, it can be seen that during the process from 0 to 10 d delay, the APV begins to correlate with the Northern Hemisphere's tropospheric westerlies on the 6th day, and by the 10th day, there is a correlation with the Southern Hemisphere's westerlies. Supplementary figure S11 shows the correlation distribution of the February Northern Hemisphere mid-to-high latitude tropospheric westerly changes with the global zonal mean zonal wind at 0, 2, 4, 6, 8, and 10 d lag. It is observed that during the process from 0 to 10 d delay (supplementary figure S11), there is no significant correlation between the Northern Hemisphere's tropospheric westerly changes and the lagged APV. Supplementary figures S10 and S11 imply that in February (when influenced by tropospheric planetary waves, leading to strong variability of the polar vortex), the connection among the APV, Northern Hemisphere tropospheric circulation, and Southern Hemisphere tropospheric circulation is more likely due to changes in the APV causing anomalous Northern Hemisphere tropospheric wave activity, which then impacts the Southern Hemisphere's atmospheric circulation through the westerly bridge.

To further substantiate the relationship between the February APV, Northern Hemisphere tropospheric circulation, and Southern Hemisphere tropospheric circulation, we employed the information flow method to investigate the causal relationships between APV, Northern Hemisphere mid-to-high latitude tropospheric westerly changes, and the global zonal wind with an 8 d lag (figures 4(c) and (d)). The impact of changes in APV can extend downwards into the troposphere after 8 d and be transmitted to the Southern Hemisphere (figure 4(c)). Meanwhile, changes in the Northern Hemisphere mid-to-high latitude tropospheric westerlies do not extend upwards into the stratosphere in the Northern Hemisphere but have a significant impact on the Southern Hemisphere (figure 4(d)).

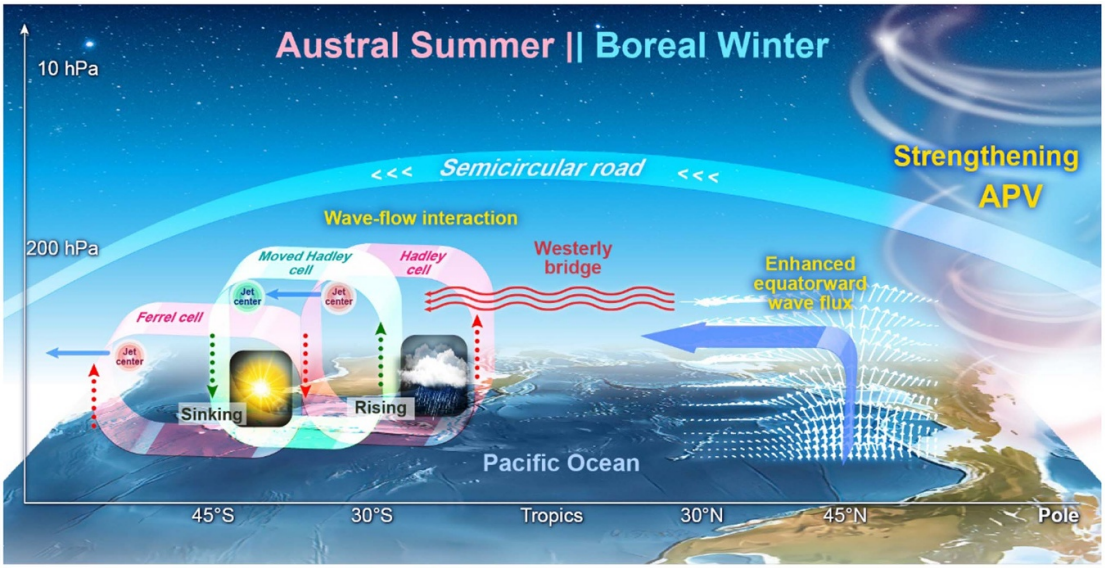

Figure 5. Schematic illustration of the mechanism by which an intensified Arctic stratospheric polar vortex influences the Southern Hemisphere. In scenarios of an intensified APV, enhanced wave activities are propelled from the Northern Hemisphere's upper troposphere to the equator during boreal winter. This is complemented by the emergence of a tropical 'westerly bridge', channeling these waves across the equator by a 'semicircular road' to impact the Southern Hemisphere's mid-to-high latitudes. The subsequent surge in the Southern Hemisphere's eddy momentum flux steers a southward shift in both the westerly jet and the Hadley cell's southern fringe. The climatic ripple effect: heightened precipitation in the subtropics and a curtailed mid-latitude rainfall during the austral summer.

4. Conclusion and discussion

In conclusion, our study uncovers that, due to the presence of the tropical westerly bridge during winter, anomalies in the Northern Hemisphere's tropospheric wave activity, induced by both strong and weak APV events, can traverse a semicircular road, exerting a pronounced influence on the Southern Hemisphere's climate. This influence is manifest as discernible shifts in wind velocity and variations in precipitation distribution. This interaction mechanism is schematically depicted in figure 5. During a strong APV event, there's a marked reduction in the upward propagation of waves from the Northern Hemisphere's troposphere to the stratosphere. This suppression allows a larger contingent of waves to venture towards the equator, cross it via the westerly bridge, and subsequently infiltrate the Southern Hemisphere. This sequence instigates an enhanced eddy momentum flux within the Southern Hemisphere, compelling a southward migration of both the westerly jet and the southern boundary of the Hadley cell. Consequently, this dynamism results in an upsurge of precipitation in the subtropics and a decline at the mid-latitudes of the Southern Hemisphere. In contrast, a weak APV event catalyzes a northward drift of the westerly jet and the southern boundary of the Hadley cell, precipitating a drop in subtropical rainfall and an elevation in mid-latitude precipitation. While it is well-established that APV exerts a considerable sway over surface climate modulations in the Northern Hemisphere, our study offers novel perspectives on the transhemispheric ramifications of APV irregularities on the Southern Hemisphere. Furthermore, it accentuates the imperative of ongoing scrutiny into the complex choreography of Earth's atmospheric interactions. If that's the case, the nonexistence of the equatorial westerly bridge during the austral winter may potentially hinder the influence of the Antarctic stratospheric polar vortex on the atmospheric circulation of the Northern Hemisphere. For detailed insights into why this relationship predominantly manifests in February and March, and the potential influence of ENSO, please see the following.

In the central and eastern Pacific, the presence of the westerly bridge spans from January to March, as evidenced in supplementary figure S12. Our correlation studies reveal that the correlation between the APVI and alterations in the Southern Hemispheric westerly jet emerges distinctly in February and March (figures 1(b) and (c)). Remarkably, January exhibits no statistically significant correlation, as demonstrated in January (figure 1(a)). The variations of the Southern Hemisphere's westerly jet during the austral summer seem to be modulated by the temperature fluctuations within the Southern Hemispheric polar vortex (Gillett and Thompson 2003, Perlwitz *et al* 2008, Son *et al* 2008). Our analysis discerns that the temperature variability of the polar vortex in January (supplementary figure S13(a)) markedly outstrips that in February and March (supplementary figure S13(b) and (c)). As an upshot, in January (supplementary figure S13(d)), the perturbations

in the Southern Hemispheric westerly jet correlate more robustly with the temperature of the Southern Hemispheric polar vortex, compared to those in February and March (supplementary figures S13(e) and (f)). This implies a dominant role of the Southern Hemispheric polar vortex temperature in modulating January's westerly jet shifts (supplementary figure S13(d)), effectively overshadowing the potential influences of APV variability.

The first EOF1 of February's zonal wind in the Southern Hemisphere (spanning 30° S–90° S) and the simultaneous time variation mode (principal component, PC1) are delineated in supplementary figure S14. This EOF1 mode of the Southern Hemispheric zonal wind mirrors the canonical 'annular mode' pattern (Limpasuvan and Hartmann 2000, Thompson and Wallace 2000). The correlation of the PC1 of this archetype with the APVI yields a value of 0.42, confidently surpassing the 95% confidence threshold. This underscores that the February zonal wind circulations in the Southern Hemisphere maintain a substantive association with APV intensity variations. In the January timeframe, the principal component analysis for zonal wind portrays the first and second modes in supplementary figure S15 (depicted as gray traces). These modes harmonize with fluctuations in the Southern Hemispheric polar vortex temperature (as represented by the red trace in supplementary figure S15(a)) and APVI (blue trace in supplementary figure S15(b)), registering correlation coefficients of 0.55 and 0.50, respectively. This analytical concurrence ratifies our earlier premise: in January, the Southern Hemispheric polar vortex temperature stands as the principal determinant of the westerly jet's shifts, with APV intensity playing a secondary role in shaping zonal wind perturbations.

ENSO and the stratospheric Quasi-Biennial Oscillation (QBO) substantially influence the intensity of APV and changes in the Southern Hemispheric westerly jet (Holton and Tan 1980, Garreaud and Battisti 1999, Manzini *et al* 2006, Garfinkel and Hartmann 2007). To eliminate these impacts, we subtracted the components linked to changes in ENSO, and QBO from the zonal wind alterations. We then recalculated the correlation coefficients between APVI and zonal wind (supplementary figure S16). The results suggest that the relationship between APVI and changes in the Southern Hemispheric westerly jet may be independent of these factors, as removing the ENSO and QBO signals had minimal impact on the outcomes.

Data availability statements

ERA5 data are available at www.ecmwf.int/en/forecasts/dataset/ecmwf-reanalysis-v5; JRA-55 data are available at https://climatedataguide.ucar.edu/climate-data/jra-55. The GPCP data are available at https://climatedataguide.ucar.edu/climate-data/gpcp-monthly-global-precipitation-climatology-project; the sensitivity experimental outputs supporting this article are available at https://doi.org/10.5281/zenodo.10055154. The bespoke code used for data analysis in this research is accessible through the corresponding author, provided that the request is reasonable.

The data that support the findings of this study are openly available at the following URL/DOI: https://zenodo.org/records/10055154.

Acknowledgments

We express our gratitude to ERA5, JRA-55, and GPCP for granting access to their invaluable reanalysis and observational datasets. Our acknowledgment extends to NCAR for facilitating the use of the CESM2-CAM6 model. This research has been made possible through the financial support of National Key Research and Development Program of China (No. 2022YFF0801701); National Natural Science Foundation of China (Grants 42122037, 42175080, 42305075); Natural Science Basic Research Program in Shaanxi Province of China (2022JM-142).

ORCID iDs

Fei Xie https://orcid.org/0000-0003-2891-3883
Xuan Ma https://orcid.org/0000-0002-0596-0786
Jianping Li https://orcid.org/0000-0003-0625-1575
Cheng Sun https://orcid.org/0000-0003-0474-7593
Yan Xia https://orcid.org/0000-0001-8664-5325

References

Adler R F *et al* 2018 The global precipitation climatology project (GPCP) monthly analysis (New Version 2.3) and a review of 2017 global precipitation *Atmosphere* **9** 138
Afargan-Gerstman H and Domeisen D I V 2020 Pacific modulation of the North Atlantic storm track response to sudden stratospheric warming events *Geophys. Res. Lett.* **47** e2019GL085007
Ambaum M H P and Hoskins B J 2002 The NAO troposphere-stratosphere connection *J. Clim.* **15** 1969–78
Baldwin M P *et al* 2021 Sudden stratospheric warmings *Rev. Geophys.* **59** e2020RG000708
Baldwin M P and Dunkerto T J 1999 Propagation of the Arctic Oscillation from the stratosphere to the troposphere *J. Geophys. Res.* **104** 30937–46
Baldwin M P and Dunkerton T J 2001 Stratospheric harbingers of anomalous weather regimes *Science* **294** 581–4
Bell B *et al* 2021 The ERA5 global reanalysis: preliminary extension to 1950 *Q. J. R. Meteorol. Soc.* **147** 4186–227
Black R X 2002 Stratospheric forcing of surface climate in the Arctic oscillation *J. Clim.* **15** 268–77
Butler A H, Sjoberg J P, Seidel D J and Rosenlof K H 2017 A sudden stratospheric warming compendium *Earth Syst. Sci. Data* **9** 63–76
Charlton-Perez A J, Ferranti L and Lee R W 2018 The influence of the stratospheric state on North Atlantic weather regimes *Q. J. R. Meteorol. Soc.* **144** 1140–51

Domeisen D I V 2019 Estimating the frequency of sudden stratospheric warming events from surface observations of the North Atlantic Oscillation *J. Geophys. Res.* **124** 3180–94
Domeisen D I V and Butler A H 2020 Stratospheric drivers of extreme events at the Earth's surface *Commun. Earth Environ.* **1** 59
Enomoto T and Matsuda Y 1999 Rossby wavepacket propagation in a zonally-varying basic flow *Tellus* A **51** 588–602
Feldstein S B 2011 Subtropical rainfall and the Antarctic Ozone Hole *Science* **332** 925–6
Garfinkel C I and Hartmann D L 2007 Effects of the El Niño–Southern Oscillation and the Quasi-Biennial Oscillation on polar temperatures in the stratosphere *J. Geophys. Res.* **112** D19112
Garreaud R D and Battisti D S 1999 Interannual (ENSO) and interdecadal (ENSO-like) variability in the Southern Hemisphere tropospheric circulation *J. Clim.* **12** 2113–23
Gillett N P and Thompson D W J 2003 Simulation of recent Southern Hemisphere climate change *Science* **302** 273–5
Hartmann D 1981 Droughts, severe winters and sudden stratospheric warmings *Nature* **293** 97–98
Haynes P H, Marks M E, McIntyre T G, Shepherd C J and Shine K P 1991 On the 'downward control' of extratropical diabatic circulations by eddy-induced mean zonal forces *J. Atmos. Sci.* **48** 651–79
Hersbach H, Bell B, Berrisford P, Hirahara S and Thépaut J 2020 The ERA5 global reanalysis *Q. J. R. Meteorol. Soc.* **146** 1999–2049
Holton J R and Tan H-C 1980 The influence of the equatorial quasi-biennial oscillation on the global circulation at 50 mb *J. Atmos. Sci.* **37** 2200–8
Hoskins B J and Ambrizzi T 1993 Rossby wave propagation on a realistic longitudinally varying flow *J. Atmos. Sci.* **50** 1661–71
Hu D, Guan Z and Tian W 2019 Signatures of the Arctic Stratospheric Ozone in Northern Hadley Circulation Extent and subtropical precipitation *Geophys. Res. Lett.* **46** 12340–9
Kang S M, Polvani L M, Fyfe J C and Sigmond M 2011 Impact of polar ozone depletion on subtropical precipitation *Science* **332** 951–4
Kidston J, Scaife A A, Hardiman S C, Mitchell D M, Butchart N, Baldwin M P and Gray L J 2015 Stratospheric influence on tropospheric jet streams, storm tracks and surface weather *Nat. Geosci.* **8** 433–40
King A D, Butler A H, Jucker M, Earl N O and Rudeva I 2019 Observed relationships between sudden stratospheric warmings and European climate extremes *J. Geophys. Res.* **124** 13943–61
Kobayashi S *et al* 2015 The JRA-55 reanalysis: general specifications and basic characteristics *J. Meteorol. Soc. Japan* **93** 5–48
Kolstad E W, Breiteig T and Scaife A A 2010 The association between stratospheric weak polar vortex events and cold air outbreaks in the Northern Hemisphere *Q. J. R. Meteorol. Soc.* **136** 886–93
Li Y, Feng J, Li J and Hu A 2019 Equatorial bridges and barriers for stationary Rossby wave propagation *J. Clim.* **32** 6117–35
Lim E P, Hendon H H, Boschat G, Hudson D, Thompson D W, Dowdy A J and Arblaster J M 2019 Australian hot and dry extremes induced by weakenings of the stratospheric polar vortex *Nat. Geosci.* **12** 896–901
Limpasuvan V and Hartmann D L 2000 Wave-maintained annular modes of climate variability *J. Clim.* **13** 4414–29
Limpasuvan V, Hartmann D L, Thompson D W, Jeev K and Yung Y L 2005 Stratosphere-troposphere evolution during polar vortex intensification *J. Geophys. Res.* **110** D24101
Lu J, Vecchi G A and Reichler T 2007 Expansion of the Hadley cell under global warming *Geophys. Res. Lett.* **34** L06805
Ma X, Xie F, Li J, Zheng X, Tian W, Ding R, Sun C and Zhang J 2019 Effects of Arctic stratospheric ozone changes on spring precipitation in the northwestern United States *Atmos. Chem. Phys.* **19** 861–75
Manzini E, Giorgetta M A, Esch M, Kornblueh L and Roeckner E 2006 The influence of sea surface temperatures on the Northern Winter Stratosphere: ensemble simulations with the MAECHAM5 model *J. Clim.* **19** 3863–81
Mitchell D M, Scott R K, Seviour W J, Thomson S I, Waugh D W, Teanby N A and Ball E R 2021 Polar vortices in planetary atmospheres *Rev. Geophys.* **59** e2020RG000723
Moulin C, Lambert C E, Dulac F and Dayan U 1997 Control of atmospheric export of dust from North Africa by the North Atlantic Oscillation *Nature* **387** 691–4
Perlwitz J, Pawson S, Fogt R L, Nielsen J E and Neff W D 2008 Impact of stratospheric ozone hole recovery on Antarctic climate *Geophys. Res. Lett.* **35** L08714
Reichler T, Kim J, Manzini E and Kröger J 2012 A stratospheric connection to Atlantic climate variability *Nat. Geosci.* **5** 783–7
Scaife A A *et al* 2022 Long-range prediction and the stratosphere *Atmos. Chem. Phys.* **22** 2601–23
Scaife A A, Folland C K, Alexander L V, Moberg A and Knight J R 2008 European climate extremes and the North Atlantic Oscillation *J. Clim.* **21** 72–83
Son S W, Polvani L M, Waugh D W, Akiyoshi H, Garcia R, Kinnison D, Pawson S, Rozanov E, Shepherd T G and Shibata K 2008 The impact of stratospheric ozone recovery on the Southern Hemisphere westerly jet *Science* **320** 1486–9
Tachibana Y, Inoue Y, Komatsu K K, Nakamura T, Honda M, Ogata K and Yamazaki K 2018 Interhemispheric synchronization between the AO and the AAO *Geophys. Res. Lett.* **45** 13477–84
Takaya K and Nakamura H 2001 A formulation of a phase-independent wave-activity flux for stationary and migratory quasigeostrophic eddies on a zonally varying basic flow *J. Atmos. Sci.* **58** 608–27
Thompson D W J, Furtado J C and Shepherd T G 2006 On the tropospheric response to anomalous stratospheric wave drag and radiative heating *J. Atmos. Sci.* **63** 2616–29
Thompson D W and Solomon S 2002 Interpretation of recent Southern Hemisphere climate change *Science* **296** 895
Thompson D W, Solomon S, Kushner P J, England M H, Grise K M and Karoly D J 2011 Signatures of the Antarctic ozone hole in Southern Hemisphere surface climate change *Nat. Geosci.* **4** 741–9
Thompson D and Wallace J 2000 Annular modes in the extratropical circulation. Part I: month-to-month variability *J. Clim.* **13** 1000–16
Tian W S, Huang J L, Zhang J K, Xie F, Wang W K and Peng Y F 2023 Role of stratospheric processes in climate change: advances and challenges *Adv. Atmos. Sci.* **40** 1379–400
Waugh D W, Sobel A H and Polvani L M 2017 What is the polar vortex and how does it influence weather? *Bull. Am. Meteorol. Soc.* **98** 37–44
Webster P J and Holton J R 1982 Cross-equatorial response to middle-latitude forcing in a zonally varying basic state *J. Atmos. Sci.* **39** 722–33
Xie F *et al* 2016 A connection from Arctic stratospheric ozone to El Niño-Southern oscillation *Environ. Res. Lett.* **11** 124026
Xie F *et al* 2018 An advanced impact of Arctic stratospheric ozone changes on spring precipitation in China *Clim. Dyn.* **51** 4029–41
Yin J H 2005 A consistent poleward shift of the storm tracks in simulations of 21st century climate *Geophys. Res. Lett.* **32** L18701